Sources and Long-term Variability of Carbon Monoxide at Mount Kenya and in Nairobi

Leonard Kirago[1], Örjan Gustafsson[1], Samuel M. Gaita[1], Sophie L. Haslett[1], Michael J. Gatari[2], Maria E. Popa[3], Thomas Röckmann[3], Christoph Zellweger[4], Martin Steinbacher[4], Jörg Klausen[5], Christian Félix[5], David Njiru[6], and August Andersson1*

[1]Department of Environmental Science, and the Bolin Centre for Climate Research, Stockholm University, 10691 Stockholm, Sweden
[2]Institute of Nuclear Science & Technology, University of Nairobi, 31907-00100 Nairobi, Kenya
[3]Institute for Marine and Atmospheric research Utrecht (IMAU), Utrecht University, Utrecht 3584CC, The Netherlands
[4]Empa, Swiss Federal Laboratories for Materials Science and Technology, Laboratory for Air Pollution/Environmental Technology, 8600 Dubendorf, Switzerland
[5]Federal Office of Meteorology and Climatology MeteoSwiss, CH-8058 Zurich, Switzerland
[6]Kenya Meteorological Department, Nairobi, Kenya

*Correspondence to: August Andersson (august.r.andersson@gmail.com)

16 **Abstract.** Carbon monoxide (CO) concentrations in the troposphere are decreasing globally, with Africa as an
17 exception. Yet, the region is understudied, with a deficit of ground-based observations and highly uncertain CO
18 emission inventories. This paper reports multi-year observational CO data from the Mt. Kenya Global Atmosphere
19 Watch (GAW) station, as well as summertime CO isotope observations from both Mt. Kenya and Nairobi, Kenya.
20 The CO variability at Mt. Kenya is characterized by slightly increased concentrations during dry periods and a
21 strong influence of short-term pollution events While multi-year data gaps complicate decadal-scale trend analysis,
22 no overall long-term shift can be resolved. High pollution events are consistent with isotopic signal from downwind
23 savanna fires. The isotope fingerprint of CO in Nairobi indicate an overwhelming dominance (near 100%) of
24 primary emissions from fossil fuel combustion - with implications for air pollution policy. In contrast, the isotope
25 signature of CO intercepted at the large footprint Mt. Kenya region suggests at least 70% primary sourced, with a
26 predominance likely from, savanna fires in Africa. Taken together, this study provides quantitative constraints of
27 primary vs secondary CO in the eastern Africa region and in urban Nairobi, with implications for satellite-based
28 emission inventories as well as for chemical-transport and climate- modelling.

1.   Introduction

Carbon monoxide (CO) is the dominant sink for the hydroxyl radical (OH), accounting for over 50% consumption of OH in the atmosphere (Lelieveld et al., 2016). It therefore influences the atmosphere's oxidation and cleansing capacity and, by extension, chemically regulates the atmospheric lifetime and abundance of other reactive gases such as methane and halocarbons (Lelieveld et al., 2016; Zheng et al., 2019). As such, CO is an indirect greenhouse gas with a net positive warming effect on climate (Szopa et al., 2021). In addition to climate effects, CO is a precursor to the formation of ground-level ozone, with implications for human health (Chen et al., 2021; WHO, 2016; Zhang et al., 2019). Anthropogenic activities such as biomass burning and fossil fuel combustion are important contributors to the global CO budget, in addition to atmospheric reactions, e.g., oxidation of hydrocarbons (Duncan et al., 2007; Zheng et al., 2019). However, the CO source contributions, mole fractions, and atmospheric residence time are spatially variable, complicating the source-sink assessment.

Global CO levels have been declining over the past two decades, but Africa is an exception. The key source of information on CO trends in the African region is satellite-based observations that show an increase in CO mole fractions (Buchholz et al., 2021; Hedelius et al., 2021; Zheng et al., 2019). However, the ground-truthing of the satellite observations is challenged by a deficit of atmospheric observatories and scant continuous long-term observations in the region (DeWitt et al., 2019; Henne et al., 2008b; Kulmala, 2018). Exacerbating this observational deficit, regional CO emission inventories are not well-defined as the continent possesses a unique CO emission profile, different from other regions such as Europe and South Asia (Crippa et al., 2018; Dasari et al., 2022; Hedelius et al., 2021). To advance our understanding of trends in CO over Africa and its source contributions, long-term CO measurements and isotope-based source apportionment studies are required but data availability is scarce.

The isotopic composition of CO provides insights into the relative strengths of regional CO sources and atmospheric processing (Brenninkmeijer, 1993; Dasari et al., 2022; Henne et al., 2008b; Röckmann et al., 2002). A particular source of CO possesses a characteristic isotopic signature, with the isotopic composition of the ambient CO reflecting that of the combined sources, sinks, and atmospheric ageing (Brenninkmeijer and Röckmann, 1997; Dasari et al., 2022; Popa et al., 2014; Röckmann et al., 1998, 2002). For example, CO from primary sources (fossil combustion and biomass burning) has a more enriched $\delta^{18}O$ signature (above +12‰) compared to that of secondary-formed CO, e.g., from oxidation of CH_4 (at ~0‰) and non-methane hydrocarbons (NMHC), at ~2.4 ± 2.4‰ (Brenninkmeijer and Röckmann, 1997).

Additional source information can be obtained from the $\delta^{13}C$ signatures. CO formed from methane oxidation is strongly depleted in ^{13}C ($\delta^{13}C$ = -51.9 ± 1.6‰) in contrast to, for example, CO emitted from burning of C_4 plants ($\delta^{13}C$ = -14.0 ± 3.8‰), C_3 plants ($\delta^{13}C$ = -26.9 ± 4.9‰) or fossil combustion at -27.8 ± 1.5‰ (Brenninkmeijer et al., 1999). However, the kinetic isotope effect (KIE) during the CO-OH reaction (the main atmospheric CO removal mechanism) results in the enrichment of $\delta^{13}C$ by 4-5‰ and more depleted $\delta^{18}O$ signatures (by ~10‰) in the lower troposphere (Brenninkmeijer et al., 1999; Röckmann et al., 1998). Overall, isotope forensics can provide valuable data on CO emissions in remote and urban locations in Africa, especially considering that the region is largely understudied, with very few ground-based CO observations and highly uncertain emission inventories.

This study investigates the long-term trends in CO mole fractions at Mt. Kenya GAW station, a high-altitude monitoring site in equatorial East Africa well suited to intercept the regional emission footprint. Online CO mole fractions measurements have been going on at the observatory since 2002, albeit with large data gaps due to technical challenges. Flask-based measurements carried out at Mt. Kenya at different periods by NOAA (2003-2011) were used for gap filling. The online and NOAA flask-measured CO data were obtained from the WMO's World Data Centre for Greenhouse Gases (WDCGG) database. After the CO measurements from Cape Point, South Africa, this is likely the longest-running data available in sub-Saharan Africa and provides observational constraints of the region's long-term trend in CO. The present study additionally provides stable isotope composition data of CO to resolve source attribution of the observed higher summertime CO amount fraction. Furthermore, the data are compared to previously obtained and unpublished isotope data fromMt. Kenya (1996-1997; earlier unpublished work by Röckmann and Brenninkmeijer) and that of an urban site in Nairobi in summer 2021 to provide further insights into regional CO sources. This dataset is unprecedented in the region and facilitates imporved understanding of the regional CO emission trends and source attribution.

2. Methodology

2.1 Measurement sites

Ambient air sampling was conducted at a remote mountain site, the Mt. Kenya Global Atmospheric Watch (GAW) station, and in Nairobi city. The Mt. Kenya GAW station is located on the north-western slope of Mt. Kenya (0.062 °S, 37.297 °E, at 3678 m MSL) in eastern equatorial Africa. The station description, site selection and representativeness, and meteorological characterization are detailed by Henne et al. (2008a, 2008b). In brief, the station lies within a nature conservancy, the Mount Kenya National Park, and contributes to the World Meteorological Organization GAW programme. The closest human settlements and roadways are over 17 km away, and the nearest town (Nanyuki) is at 1900 m MSL. A small touristic infrastructure, the Old Moses Camp, is situated 300 m below and ca. 1.9 km to the NNW of the station. The second site, in the megacity of Nairobi, Kenya, was a rooftop measurement site (~17 m above ground level; 1690 m asl.; 1.279° S, 36.817° E). As described previously, the Nairobi site is representative of the city's ambient conditions (Kirago et al., 2022b).

2.2 Ambient air sampling

Glass flask sampling was conducted in August 2021 at the Mt. Kenya GAW station and in Nairobi with an in-house assembled portable sampler consisting of a diaphragm pump (KNF Neuberger N86E) connected with 1/4" Dekabon tubing. The sampler design, glass flask pre-conditioning protocol and sampling procedure are previously described (Dasari et al., 2022). Briefly, the sampler was designed to fill two pre-conditioned glass flasks (Normag, 1L) simultaneously. Ambient air was drawn at a flow rate of 2 L min^{-1} and dried through a magnesium perchlorate trap. First, the glass flasks were flushed for 20 minutes before compressing the dried air to an absolute pressure of ~1.7 bar. At Mt. Kenya GAW station, 21 nighttime (02:00h local time) and six daytime (14:00h local time) air sample sets were collected. Nine sample pairs were collected in Nairobi (every second day; daytime only; 14:00h local time). The filled glass flasks were sent to the Institute for Marine and Atmospheric Research Utrecht (IMAU), Utrecht University, for processing and stable isotope analysis of CO.

102   **2.3**   **Measurements of CO mole fractions and stable isotopes ($\delta^{18}O$ and $\delta^{13}C$) composition of CO**

103   The CO mole fraction and stable isotopic composition measurements of the collected glass flask samples were

104   performed at IMAU, Utrecht University. A continuous-flow isotope ratio mass spectrometry (CF-IRMS, Thermo

105   Scientific Delta V Advantage) system was used, applying a previously described measurement protocol (Pathirana

106   et al., 2015). In brief, the sample gas was introduced into the analytical system using an automated multi-port unit,

107   via a mass flow controller and under ultra-high-purity helium flow. Here, the air sample was directed through a

108   trap with Ascarite (8 - 20 mesh, Thermo Scientific™) followed by magnesium perchlorate (Sigma-Aldrich), to

109   remove CO_2 and water. A subsequent cryogenic trap (liquid N_2, -196 °C) was used to remove the remaining traces

110   of CO_2, N2O and hydrocarbons. The CO in the clean air matrix was then oxidized to CO_2 using Schütze reagent

111   (I_2O_5/H_2SO_4 mixture on granular silica gel) synthesized in-house. Subsequently, the CO-derived CO_2 was cryo-

112   trapped in liquid-N_2, while other residual gases (e.g., O_2 and N_2) were pumped out. The sample was further purified

113   on a GC column, dried via a Nafion dryer, and subsequently transferred to the CF-IRMS via an open split inlet for

114   stable isotopes ($\delta^{18}O$ and $\delta^{13}C$) analysis.(Pathirana et al., 2015) The original CO amount fraction was deduced

115   from the quantity of the derived CO_2.

116   The isotopic composition is expressed as per mil (‰) enrichment or depletion of the isotope ratio in the sample

117   relative to that of international standard materials, which in these cases are the Vienna PeeDeeBelemnite (V-PDB)

118   standard for $\delta^{13}C$-CO, and the Vienna Standard Mean Ocean Water (V-SMOW) for $\delta^{18}O$-CO measurements

119   (Brenninkmeijer et al., 1999; Pathirana et al., 2015). A reference cylinder with atmospheric air with known isotopic

120   composition and mole fraction ($\delta^{13}C$ = -30.25‰; $\delta^{18}O$ = +7.10‰; CO = 180 ppb) was used for calibration.

121   Periodical measurements of "target" gases were used to monitor the precision and accuracy of the measurements,

122   as well as the long-term stability of the analytical system (Pathirana et al., 2015). In addition, blank runs (without

123   injecting the sample or reference gas) were performed to assess the background CO_2, mainly from the Schütze

124   reagent. The typical 1-sigma measurement reproducibility during the time of these analyses is estimated at 0.12‰

125   for $\delta^{13}C$ and 0.16‰ for $\delta^{18}O$.

126   **2.4**   **Sampling and isotopic characterization of CO for the 1996/97 campaign**

127   The 1996/97 high-volume air samples were collected on an exploratory mission around Mount Kenya following

128   the ring road A2/B6, and branching off towards the mountain to locations where sufficient power was available

129   for sample collection. During this campaign and later incidental samplings, air samples of approximately 500 L

130   volume were compressed into 5 L aluminium cylinders using a modified RIX compressor (Mak and

131   Brenninkmeijer, 1994). Unfortunately, records of precise locations have been lost. The filled cylinders were sent

132   to the Max Planck Institute for Chemistry in Mainz, Germany, for CO isotope analysis on a high-volume extraction

133   unit (Brenninkmeijer et al., 1999; Röckmann et al., 2002). A high CO concentration calibration gas (269 ppm) that

134   was used during the 1996/7 measurements has been preserved and is regularly measured in the lab of Utrecht

135   University to assure scale compatibility.

136

137   **2.5   Long-term CO mole fractions at the Mt. Kenya GAW station**

138   High-resolution CO data from Mt. Kenya GAW station are available from the WMO World Data Centre for
139   Greenhouse Gases (WDCGG; https://gaw.kishou.go.jp/). A continuous time series is available for the 2002-2006
140   and 2020-2021 periods, with some large gaps attributable mainly to power outages and data quality issues.
141   Between 2010 and 2015, the station was disconnected from the power grid following a bush fire, while
142   performance audits revealed the CO analyzer to be in poor working condition between 2015-2019
143   (decommissioned in 2020), compromising the data quality (Zellweger et al., 2020). Over time, the CO
144   measurements were made using different CO analyzers (Thermo Electron Corporation TEI 48C-TL in 2002-2006,
145   Horiba APMA360 in 2010-2019, and Picarro G2401 in 2020-2021).

146   The instrument calibration, quality control protocols, and data treatment procedures are discussed elsewhere
147   (Henne et al., 2008b; Zellweger et al., 2009, 2020). In brief, ambient air was drawn into the CO instrument using
148   1/4" Teflon (till 2019) and ¼" Synflex 1300 (after 2019) tubings at a flow rate of 4 l/min via a Nafion drier to
149   remove moisture and a particle filter. The air inlet was about 7 m above ground and protected against rain, snow
150   and direct wind. These instruments were installed and calibrated by the Swiss Federal Institute for Materials
151   Science and Technology (Empa) in collaboration with the Federal Office of Meteorology and Climatology
152   MeteoSwiss, and operated by the Kenya Meteorological Department (KMD). The instrument calibration and
153   performance audits are conducted regularly by the GAW World Calibration Center hosted at Empa (Zellweger et
154   al., 2020).

155   **2.6   Trajectory and statistical modelling**

156   The air mass back trajectories (10 days; arrival height of 100 m above ground level) were calculated to identify
157   the air mass source region. The NOAA Hybrid Single-Particle Lagrangian Integrated Trajectory model (HYSPLIT,
158   version 4) and GDAS (1º × 1º) archived meteorological datasets were used (Stein et al., 2015). The Bayesian
159   Markov chain Monte Carlo (MCMC) model was used to quantitatively constrain CO fractional contributions and
160   account for source end member variability and measurement uncertainties (Dasari et al., 2022). The MCMC
161   simulations were carried out with MATLAB R2020 with 1,000,000 runs and 10,000 runs for sample burn-in and
162   a data thing of 100.

163   **3.   Results and Discussion**

164   **3.1   CO mole fractions at Mt. Kenya GAW Station**

165   The results of the continuous CO observations at Mt. Kenya GAW station, both online and flask measurements,
166   are presented in Figure 1. Part of the data (2002 - 2006) has been comprehensively discussed previously (Henne
167   et al., 2008b), and here it will be only compared to the 2021 period with respect to a general long-term trend.
168   Overall, peak CO mole fractions were observed during the dry periods (SI Figure S1). However, the seasonal
169   variations are not pronounced; the intra-seasonal peak-to-peak amplitude is larger than the variations between
170   different seasons, implying a strong influence of short-term pollution events. Meanwhile, no clear multi-year trend

171   in CO concentrations were detected (the rate of the long-term trend is ~ 0 ppb/year), albeit the large data gaps and

172   different measurement techniques precludes a detailed analysis.

173   The observed CO levels, ranging between 55 – 250 ppb, are comparable to those previously recorded at Mt. Kenya

174   station (Henne et al., 2008b), but lower than CO concentrations reported at the Rwanda Climate Observatory -

175   another remote site also in Eastern Africa, possibly with a stronger and more direct influence of savanna burning

176   episodes (DeWitt et al., 2019). Overall, changes in source strength, airmass transport pathways and meteorological

177   parameters such as planetary boundary layer thickness are likely to be key drivers of the observed temporal

178   variations.

179   Back-trajectories calculated with the HYSPLIT model were combined with the CO data to learn more about source

180   regions incident with elevated CO mole fractions. Air masses originating from different geographical areas, such

181   as from eastern Africa, Arabian Peninsula, northern Africa, South Asia, and south-eastern Africa, as well as cleaner

182   air masses from the Indian Ocean, are intercepted at Mt. Kenya GAW station (Figure 2). This underlines the

183   suitability of Mt. Kenya GAW station to capture both the regional and intercontinental footprints. The elevated

184   summertime (June - August) CO mole fractions are linked to the arrival of south-easterly airmasses, coinciding

185   with large-scale savanna fires in southern Africa and Madagascar. The air masses shift north-easterly during winter

186   (December - March), and coincide with savanna fires in northern Africa (Andersson et al., 2020; Kirago et al.,

187   2022a). Although the intercepted air masses do not directly flow over West-Central Sub-Saharan Africa, where

188   most fires occur, the atmospheric residence time of CO is sufficient for regional and intercontinental mixing. Air

189   masses with elevated CO loadings from South Asia and the Arabian Peninsula are also intercepted during winter.

190   High wintertime CO amount fractions have been reported from a South Asian receptor site in the northern Indian

191   Ocean (Dasari et al., 2022). Taken together, the seasonal variability in CO mole fraction can partly be explained

192   by regional emission events, combined with a contribution from other geographical source regions such as South

193   Asia.

194   **3.2   Isotopic constraints of sources to CO from Mount Kenya and Nairobi**

195   The stable isotope composition of CO ($\delta^{13}C$ and $\delta^{18}O$) for ambient samples from Mt. Kenya GAW station during

196   August 2021 varied temporally and inversely with the CO mole fractions. The $\delta^{13}C$ ranged between -31.5‰ to -

197   28.0‰, while $\delta^{18}O$ ranged between 2.5 to 10.0‰ (SI Figure S2). However, there were no distinct temporal or

198   diurnal trends in the recorded isotopic values (both daytime and night-time samples were measured). The air

199   masses were consistently southeasterly during the three weeks study period (SI Figure S3). Comparable $\delta^{18}O$

200   composition was observed in 1996/97 samples (ranged between 3.7 to 10.4‰), but was more enriched in $\delta^{13}C$ (-

201   28.4‰ to -26.6‰). The isotopic composition in the Mt. Kenya background region was distinct from that of the

202   urban Nairobi location that recorded highly enriched $\delta^{18}O$ values (17.5 ± 2.2‰; SI Figure S2).

203   The Keeling plot approach provides insights into the regional CO sources. Here, a linear relationship is observed

204   between the isotope signatures and the inverse of the CO amount fractions ($\delta^{13}C$ vs 1/[CO] and $\delta^{18}O$ vs 1/[CO])

205   both at Mt. Kenya and in Nairobi (Figure 3). This implies that the CO dynamics in this system can be described

206   by a two-component mixture; a relatively stable background fraction and a regional source. The y-axis intercept

207   in this relation represents the source signature. At Mt. Kenya, analysis of the recently-obtained dataset (2021)

208   reveals the stable isotopes signature of the source of $\delta^{18}O = 14.0 \pm 1.2‰$ and $\delta^{13}C = -27.7 \pm 0.6‰$. For the samples

209   collected during the 1996/97 campaign, the $\delta^{18}O$ signature is very similar and indistinguishable ($\delta^{18}O = 14.2 \pm$

210   2.1‰), while the source is more enriched in ^{13}C ($\delta^{13}C = -24.7 \pm 0.7‰$; Figure 4). The latter suggests differences

211   in the relative strengths of the contributing sources, possibly a relatively higher contribution from C_4 plants burning

212   or a relatively smaller influence of secondary CO from atmospheric reactions during the 1996/97 campaign It

213   should be kept in mind that the 1990s samples were obtained at a lower altitude location on the slopes of Mt Kenya.

214   C_4 plants like maize and sugarcane are commonly grown in Kenya, while also biomass usage (including crop

215   residuals for household energy) and agricultural burning are prevalent in the region (World Bank, 2011). In

216   Nairobi, a clearly distinct source signature is noted, especially for $\delta^{18}O$ ($\delta^{13}C = -26.0 \pm 0.4‰$ and $\delta^{18}O = 22.9 \pm$

217   0.8‰; Figures 4). The highly enriched $\delta^{18}O$ source signature in Nairobi indicates almost exclusively high

218   temperature combustion sources, while a mixed source regime (both combustion sources and CO emanating from

219   atmospheric reactions) is observed at Mt. Kenya; these can be quantitatively resolved using an isotopic mass

220   balance approach

221   The source signatures can be used to quantitatively constrain the fractional contributions of CO in the regional

222   background and urban atmosphere (Dasari et al., 2022). However, information was available for only two isotopes,

223   $\delta^{13}C$ and $\delta^{18}O$, against five potential sources that can contribute to the overall CO isotopic signature (C_3 plants,

224   fossil, C_4 plants, CH_4 oxidation and NMHC oxidation), yielding a mathematically under-determined scenario.

225   Furthermore, the weak linear correlation for $\delta^{13}C$ in the Keeling plot ($\delta^{13}C$ vs $1/[CO]$; $R^2 = 0.34$ for Mt. Kenya)

226   limits its application in the statistical model. Therefore, only $\delta^{18}O$ signatures were here modelled ($R^2 = 0.64$ for

227   both Mt. Kenya; $R^2 = 0.89$ for Nairobi; $P <0.05$). Hence, the CO sources were partitioned into two major classes:

228   primary/combustion (fossil, C_3 and C_4 biomass) and secondary (i.e., oxidation of methane and NMHC).

229   A Bayesian statistical model, drawing upon the model described in Dasari et al. (2022), was used to estimate the

230   contribution of secondary ($f_{secondary}$) vs primary ($f_{primary}$) CO sources. In this model the relative contributions of

231   primary vs. secondary CO for the temporally varying source is computed, corresponding to the $\delta^{18}O$ values at the

232   limit where $1/CO$ approaches zero (the $\delta^{18}O$ intercept in the Keeling plot). First, the source end members for the

233   two fractions were established. Unlike the oxidation of NMHC, the CH_4-oxidized CO fluxes have little variability

234   (CH_4 has a long atmospheric lifetime) and largely contribute to the background signal (Dasari et al., 2022; Worden

235   et al., 2019; Zheng et al., 2019). Therefore, the temporally-varying secondary CO end member was assigned that

236   of the NMHC oxidation source ($\delta^{18}O_{secondary} = 2.4 \pm 2.4‰$).

237   The primary CO end member is a composite of the three combustion sources; C_4 biomass ($+20.2 \pm 4.9‰$), C_3

238   biomass ($+16.3 \pm 5.1‰$) and fossil fuel combustion at $+19.2 \pm 4.9‰$ (Dasari et al., 2022). Although the relative

239   contributions are uncertain, the $\delta^{18}O$ end members largely overlap. Model estimates show biomass burning in

240   Africa accounts for 80 - 90% of the surface CO emissions (Zheng et al., 2018). Similar contributions to black

241   carbon (different but co-emitted incomplete combustion product) were observed using isotopic constraints with

242   near-equal contributions from C_3 and C_4 biomass in the eastern Africa background atmosphere (Kirago et al.,

243   2022c). Therefore, the relative source contributions were estimated at 50% from C_3 biomass and 50% from C_4 and

244   fossil sources at Mt. Kenya. Hence, a primary CO end member was established at $\delta^{18}O_{primary} = 18.4 \pm 3.5‰$. In

245   Nairobi, fossil fuel combustion was estimated to contribute to 85% of the CO emission in the city ($\delta^{18}O_{primary} =$

246 +19.2 ± 4.9‰). Since individual source end members in the primary fraction largely overlap, the model simulations

247 were generally insensitive to chosen priors, as investigated by sensitivity analysis.

248 A similar $\delta^{18}O$ source signature (~14.0 ± 2.1‰) was observed at the two Mt. Kenya campaigns (1996/97 and

249 2021). Applying the established endmembers, we estimate the contribution of CO from primary/ combustion

250 sources at the regional background site to be at least 70%. In contrast, we found an almost exclusively primary CO

251 component for the urban Nairobi case. Nairobi is a strong air pollution source region, and the CO loadings largely

252 reflect the city's CO emissions. CO is, e.g., a precursor to low-level ozone, and thus emissions deteriorate air

253 quality. Present findings show that air quality policy should target primary emissions, especially from traffic

254 (Kirago et al., 2022b). In contrast, Mt. Kenya GAW station captures a more regional footprint with a dominant

255 contribution from savanna fires.

256 **4.   Conclusion**

257 This study provides ground-observational constraints that broadly supports earlier suggestions that savanna fires

258 are the main emitters and modulators of CO loadings over Sub-Saharan Africa. Albeit data gaps in CO mixing

259 ratios prevent detailed analysis, no clear long-term trend was resolved for the Mt. Kenya GAW station. Isotope-

260 based source apportionment shows that at least two thirds of the CO emitted from East African savanna fires are

261 of primary origins, while for Nairobi primary sources approach 100%. The latter has implications for air quality

262 policy, suggesting primary emissions such as traffic should be targeted, in line with previous findings for BC

263 (Kirago et al., 2022b). These findings put constraints on satellite-based emission inventories and chemical-

264 transport and climate modelling. Overall, this study corroborates earlier findings that in order to reduce the

265 secondary climate warming effect from CO over Sub-Saharan Africa, man-made savanna fires should be reduced

266 (Andersson et al., 2020).

267 **Acknowledgement**

268 This work was supported by research grants from the Swedish Research Council (VR contracts nos. 2013-114,

269 2017-05687 and 2020-05384), the Swedish Research Council for Sustainable Development (FORMAS contract

270 no. 2020-01951), and the Swedish Research Council Distinguished Professor Grant (VR contract no. 2017-

271 01601). Sample analysis was supported by the research grants from European Commission under the Horizon

272 2020 – Research and Innovation Framework Programme, H2020-INFRAIA-2020-1 (grant agreement number

273 101008004).

274 We commend the efforts of the Kenya Meteorological Department (KMD), the Swiss Federal Institute for

275 Materials Science and Technology (Empa), and the Federal Office of Meteorology and Climatology MeteoSwiss

276 for Mt. Kenya GAW Station operations. We appreciate the field and technical support from the staff at the Institute

277 of Nuclear Science & Technology, University of Nairobi and KMD. We commend Prof. Carl Brenninkmeijer and

278 Sergey Gromov for their contribution to science, and contribution to 1996/97 campaign/ data used in this

279 manuscript.

280   We acknowledge the use of data from the World Data Centre for Greenhouse Gases (WDCGG) database
281   (https://gaw.kishou.go.jp/), hosted by the World Meteorological Organization. The authors gratefully acknowledge
282   the NOAA Air Resources Laboratory (ARL) for the provision of the HYSPLIT transport and dispersion model
283   and/or READY website (https://www.ready.noaa.gov) used in this publication.

284   **Author Contribution**

285   Conceptualization of the study by AA and ÖG. Design and execution of field campaigns by LK, AA, SG and MJG.
286   Management of Mt. Kenya GAW station and instrument calibration by DN, JK, CZ, CF & MS. Isotope analysis
287   by MEP. 1996/97 sampling campaign and sample analysis by TR. Data analysis by LK with support from AA,
288   ÖG, SLH and SG; Manuscript writing by LK with support from co-authors.

289   **Competing interests**

290   The authors declare no competing interests.

291   **References**

292   Andersson, A., Kirillova, E. N., Decesari, S., Dewitt, L., Gasore, J., Potter, K. E., Prinn, R. G., Rupakheti, M., De
293   Dieu Ndikubwimana, J., Nkusi, J. and Safari, B.: Seasonal source variability of carbonaceous aerosols at the
294   Rwanda Climate Observatory, Atmos. Chem. Phys., 20(8), 4561–4573, doi:10.5194/acp-20-4561-2020, 2020.

295   Brenninkmeijer, C. A. M.: Measurement of the abundance of 14CO in the atmosphere and the 13C/12C and
296   18O/16O ratio of atmospheric CO with applications in New Zealand and Antarctica, J. Geophys. Res., 98(D6),
297   doi:10.1029/93jd00587, 1993.

298   Brenninkmeijer, C. A. M. and Röckmann, T.: Principal factors determining the 18O/16O ratio of atmospheric CO
299   as derived from observations in the southern hemispheric troposphere and lowermost stratosphere, J. Geophys.
300   Res. Atmos., 102(21), 25477–25485, doi:10.1029/97jd02291, 1997.

301   Brenninkmeijer, C. A. M., Röckmann, T., Bräunlich, M., Jöckei, P. and Bergamaschi, P.: Review of progress in
302   isotope studies of atmospheric carbon monoxide, Chemosph. - Glob. Chang. Sci., 1(1–3), 33–52,
303   doi:10.1016/S1465-9972(99)00018-5, 1999.

304   Buchholz, R. R., Worden, H. M., Park, M., Francis, G., Deeter, M. N., Edwards, D. P., Emmons, L. K., Gaubert,
305   B., Gille, J., Martínez-Alonso, S., Tang, W., Kumar, R., Drummond, J. R., Clerbaux, C., George, M., Coheur, P.
306   F., Hurtmans, D., Bowman, K. W., Luo, M., Payne, V. H., Worden, J. R., Chin, M., Levy, R. C., Warner, J., Wei,
307   Z. and Kulawik, S. S.: Air pollution trends measured from Terra: CO and AOD over industrial, fire-prone, and
308   background regions, Remote Sens. Environ., 256, 112275, doi:10.1016/j.rse.2020.112275, 2021.

309   Chen, K., Breitner, S., Wolf, K., Stafoggia, M., Sera, F., Vicedo-Cabrera, A. M., Guo, Y., Tong, S., Lavigne, E.,
310   Matus, P., Valdés, N., Kan, H., Jaakkola, J. J. K., Ryti, N. R. I., Huber, V., Scortichini, M., Hashizume, M., Honda,
311   Y., Nunes, B., Madureira, J., Holobâcă, I. H., Fratianni, S., Kim, H., Lee, W., Tobias, A., Íñiguez, C., Forsberg,
312   B., Åström, C., Ragettli, M. S., Guo, Y. L. L., Chen, B. Y., Li, S., Milojevic, A., Zanobetti, A., Schwartz, J., Bell,

313   M. L., Gasparrini, A. and Schneider, A.: Ambient carbon monoxide and daily mortality: a global time-series study

314   in 337 cities, Lancet Planet. Heal., 5(4), e191–e199, doi:10.1016/S2542-5196(21)00026-7, 2021.

315   Crippa, M., Guizzardi, D., Muntean, M., Schaaf, E., Dentener, F., Van Aardenne, J. A., Monni, S., Doering, U.,

316   Olivier, J. G. J., Pagliari, V. and Janssens-Maenhout, G.: Gridded emissions of air pollutants for the period 1970-

317   2012 within EDGAR v4.3.2, Earth Syst. Sci. Data, 10(4), 1987–2013, doi:10.5194/essd-10-1987-2018, 2018.

318   Dasari, S., Andersson, A., Popa, M. E., Röckmann, T., Holmstrand, H., Budhavant, K. and Gustafsson, Ö.:

319   Observational Evidence of Large Contribution from Primary Sources for Carbon Monoxide in the South Asian

320   Outflow, Environ. Sci. Technol., 56(1), 165–174, doi:10.1021/acs.est.1c05486, 2022.

321   DeWitt, H. L., Gasore, J., Rupakheti, M., Potter, K. E., Prinn, R. G., De Dieu Ndikubwimana, J., Nkusi, J. and

322   Safari, B.: Seasonal and diurnal variability in O3, black carbon, and CO measured at the Rwanda Climate

323   Observatory, Atmos. Chem. Phys., 19(3), 2063–2078, doi:10.5194/acp-19-2063-2019, 2019.

324   Duncan, B. N., Logan, J. A., Bey, I., Megretskaia, I. A., Yantosca, R. M., Novelli, P. C., Jones, N. B. and Rinsland,

325   C. P.: Global budget of CO, 1988 - 1997: Source estimates and validation with a global model, J. Geophys. Res.

326   Atmos., 112(22), 1988–1997, doi:10.1029/2007JD008459, 2007.

327   Hedelius, J. K., Toon, G. C., Buchholz, R. R., Iraci, L. T., Podolske, J. R., Roehl, C. M., Wennberg, P. O., Worden,

328   H. M. and Wunch, D.: Regional and Urban Column CO Trends and Anomalies as Observed by MOPITT Over

329   16 Years, J. Geophys. Res. Atmos., 126(5), 1–18, doi:10.1029/2020JD033967, 2021.

330   Henne, S., Junkermann, W., Kariuki, J. M., Aseyo, J. and Klausen, J.: Mount Kenya global atmosphere watch

331   station (MKN): Installation and meteorological characterization, J. Appl. Meteorol. Climatol., 47(11), 2946–2962,

332   doi:10.1175/2008JAMC1834.1, 2008a.

333   Henne, S., Klausen, J., Junkermann, W., Kariuki, J. M., Aseyo, J. O. and Buchmann, B.: Representativeness and

334   climatology of carbon monoxide and ozone at the global GAW station Mt. Kenya in equatorial Africa, Atmos.

335   Chem. Phys., 8(12), 3119–3139, doi:10.5194/acp-8-3119-2008, 2008b.

336   Kirago, L., Gustafsson, Ö., Gaita, S. M., Haslett, S. L., deWitt, H. L., Gasore, J., Potter, K. E., Prinn, R. G.,

337   Rupakheti, M., Ndikubwimana, J. de D., Safari, B. and Andersson, A.: Atmospheric Black Carbon Loadings and

338   Sources over Eastern Sub-Saharan Africa Are Governed by the Regional Savanna Fires, Environ. Sci. Technol.,

339   doi:10.1021/acs.est.2c05837, 2022a.

340   Kirago, L., Gatari, M. J., Gustafsson, Ö. and Andersson, A.: Black carbon emissions from traffic contribute

341   substantially to air pollution in Nairobi, Kenya, Commun. Earth Environ., 3(1), 1–8, doi:10.1038/s43247-022-

342   00400-1, 2022b.

343   Kirago, L., Gatari, M. J., Gustafsson, Ö. and Andersson, A.: Large Contribution of Fossil Black Carbon to Air

344   Pollution in Nairobi , Kenya, Commun. Earth Environ., 2022c.

345   Kulmala, M.: Build a global Earth observatory, Nature, 553(7686), 21–23, doi:10.1038/d41586-017-08967-y,

346   2018.

347   Lelieveld, J., Gromov, S., Pozzer, A. and Taraborrelli, D.: Global tropospheric hydroxyl distribution, budget and
348   reactivity, Atmos. Chem. Phys., 16(19), 12477–12493, doi:10.5194/acp-16-12477-2016, 2016.

349   Mak, J. E. and Brenninkmeijer, C. A. M.: Compressed air sample technology for isotopic analysis of atmospheric
350   carbon   monoxide,   J.   Atmos.   Ocean.   Technol.,   11(2),   425–431,   doi:https://doi.org/10.1175/1520-
351   0426(1994)011%3C0425:CASTFI%3E2.0.CO;2, 1994.

352   Pathirana, S. L., Van Der Veen, C., Popa, M. E. and Röckmann, T.: An analytical system for stable isotope analysis
353   on carbon monoxide using continuous-flow isotope-ratio mass spectrometry, Atmos. Meas. Tech., 8(12), 5315–
354   5324, doi:10.5194/amt-8-5315-2015, 2015.

355   Popa, M. E., Vollmer, M. K., Jordan, A., Brand, W. A., Pathirana, S. L., Rothe, M. and Röckmann, T.: Vehicle
356   emissions of greenhouse gases and related tracers from a tunnel study: CO : CO2, N2O : CH4 : O2 : Atios, and the
357   stable isotopes 13C and 18O in CO2 and CO, Atmos. Chem. Phys., 14(4), 2105–2123, doi:10.5194/acp-14-2105-
358   2014, 2014.

359   Röckmann, T., Brenninkmeijer, C. A. M., Saueressig, G., Bergamaschi, P., Crowley, J. N., Fischer, H. and Crutzen,
360   P. J.: Mass-independent oxygen isotope fractionation in atmospheric CO as a result of the reaction CO + OH,
361   Science (80-.)., 281(5376), 544–546, doi:10.1126/science.281.5376.544, 1998.

362   Röckmann, T., Jöckel, P., Gros, V., Bräunlich, M., Possnert, G. and Brenninkmeijer, C. A. M.: Using 14C, 13C,
363   18O and 17O isotopic variations to provide insights into the high northern latitude surface CO inventory, Atmos.
364   Chem. Phys., 2, 147–159 [online] Available from: www.atmos-chem-phys.org/acp/2/147/, 2002.

365   Stein, A. F., Draxler, R. R., Rolph, G. D., Stunder, B. J. B., Cohen, M. D. and Ngan, F.: Noaa's hysplit atmospheric
366   transport and dispersion modeling system, Bull. Am. Meteorol. Soc., 96(12), 2059–2077, doi:10.1175/BAMS-D-
367   14-00110.1, 2015.

368   Szopa, S., Naik, V., Adhikary, B., Artaxo, P., Berntsen, T., Collins, W. D., Fuzzi, S., Gallardo, L., Kiendler, A.,
369   Scharr, Z., Klimont, Liao, H., Unger, N. and Zanis, P.: Short-Lived Climate Forcers. In Climate Change 2021: The
370   Physical Science Basis. Contribution of Working Group I to the Sixth Assessment Report of the Intergovernmental
371   Panel on Climate Change. [online] Available from: https://www.ipcc.ch/, 2021.

372   WHO: WHO Expert Consultation: Available evidence for the future update of the WHO Global Air Quality
373   Guidelines, Copenhagen, Denmark. [online] Available from: http://www.euro.who.int/pubrequest, 2016.

374   Worden, H. M., Anthony Bloom, A., Worden, J. R., Jiang, Z., Marais, E. A., Stavrakou, T., Gaubert, B. and Lacey,
375   F.: New constraints on biogenic emissions using satellite-based estimates of carbon monoxide fluxes, Atmos.
376   Chem. Phys., 19(21), 13569–13579, doi:10.5194/acp-19-13569-2019, 2019.

377   World Bank: Wood-Based Biomass Energy Development for Sub-Saharan Africa, Washington, D.C., 2011.

378 Zellweger, C., Hüglin, C., Klausen, J., Steinbacher, M., Vollmer, M. and Buchmann, B.: Inter-comparison of four

379 different carbon monoxide measurement techniques and evaluation of the long-term carbon monoxide time series

380 of Jungfraujoch, Atmos. Chem. Phys., 9(11), 3491–3503, doi:10.5194/acp-9-3491-2009, 2009.

381 Zellweger, C., Steinbacher, M. and Buchmann, B.: GAW Report No. 256 / WCC-Empa Report No. 19/4. System

382 and Performance Audit of Surface Ozone, Carbon Monoxide, Methane, and Carbon Dioxide at the Global GAW

383 Station   Mt.   Kenya,   Kenya,   Geneva.   [online]   Available   from:

384 https://library.wmo.int/index.php?lvl=notice_display&id=21780, 2020.

385 Zhang, J. J., Wei, Y. and Fang, Z.: Ozone pollution: A major health hazard worldwide, Front. Immunol., 10(OCT),

386 1–10, doi:10.3389/fimmu.2019.02518, 2019.

387 Zheng, B., Chevallier, F., Ciais, P., Yin, Y. and Wang, Y.: On the Role of the Flaming to Smoldering Transition

388 in the Seasonal Cycle of African Fire Emissions, Geophys. Res. Lett., 45(21), 11,998-12,007,

389 doi:10.1029/2018GL079092, 2018.

390 Zheng, B., Chevallier, F., Yin, Y., Ciais, P., Fortems-Cheiney, A., Deeter, M. N., Parker, R. J., Wang, Y., Worden,

391 H. M. and Zhao, Y.: Global atmospheric carbon monoxide budget 2000-2017 inferred from multi-species

392 atmospheric inversions, Earth Syst. Sci. Data, 11(3), 1411–1436, doi:10.5194/essd-11-1411-2019, 2019.
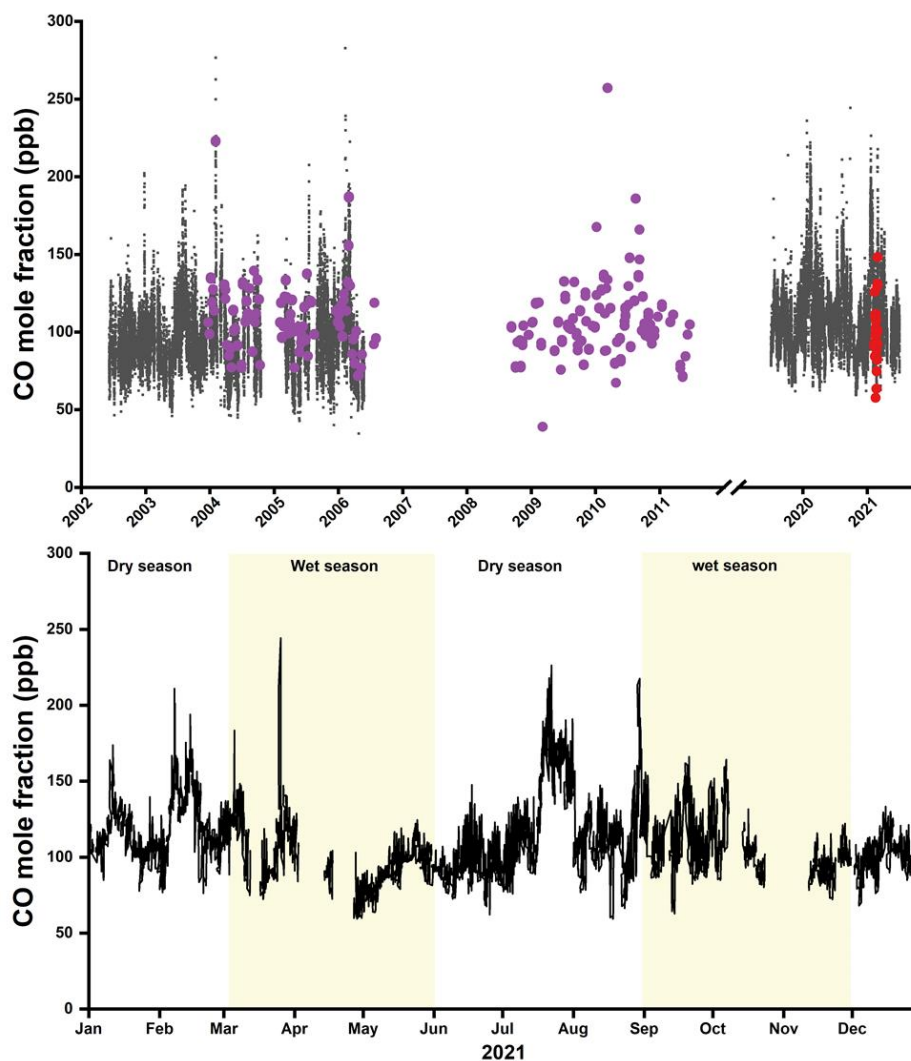
Figure 1: Time series of CO mole fractions at Mt. Kenya GAW station. a) Daily-resolution continuously measured CO mole fraction (Picarro) at Mt. Kenya GAW is represented by black dots. The CO data was retrieved from the WMO's-WDCGG database covering 2002 to 2021. Different instrumentations were used over time, but similar instrumental calibration, quality control, and assurance protocols were applied. Flask-based measurements by NOAA at the station are presented in purple symbols, while flask samples during our 2021 campaign are shown in red symbols. b) Variations in CO mole fractions for the year 2021. The prevailing typical weather conditions are indicated.
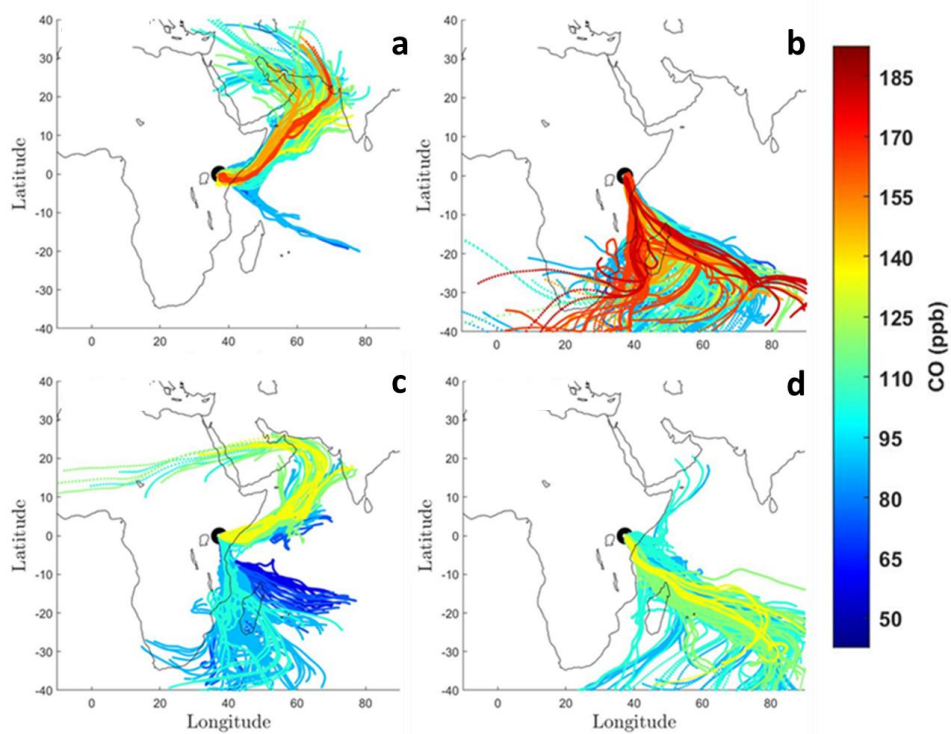
Figure 2: Seasonal changes in CO concentration-coded back trajectories intercepted at Mt. Kenya; (a) December – February, (b) June – August, (c) March – May, and (d) September – November. Ten days air masses back trajectories are calculated at an arrival height of 100 m above ground level.
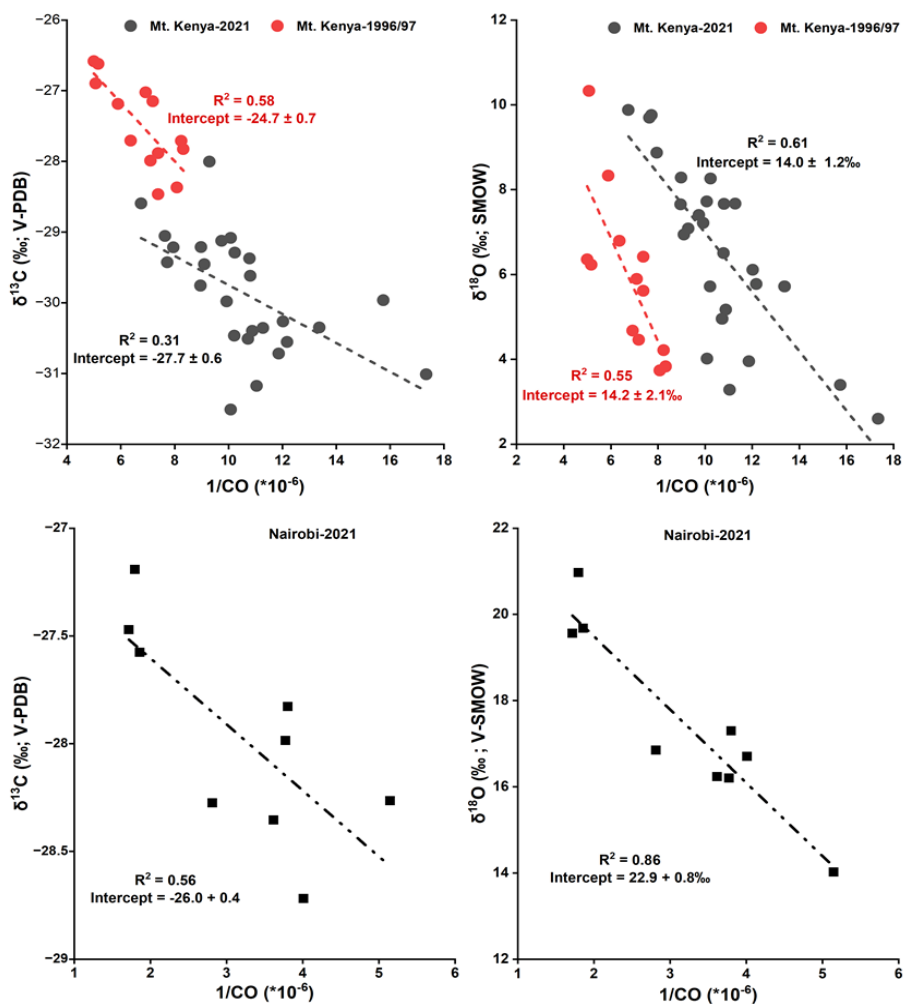
Figure 3: The Keeling relation plots (i.e., isotopic signature vs the inverse of the measured CO mole fraction) for Mt. Kenya (top panel) and Nairobi (bottom panel). The y-intercept in the Keeling relationship represents the source signature.

408
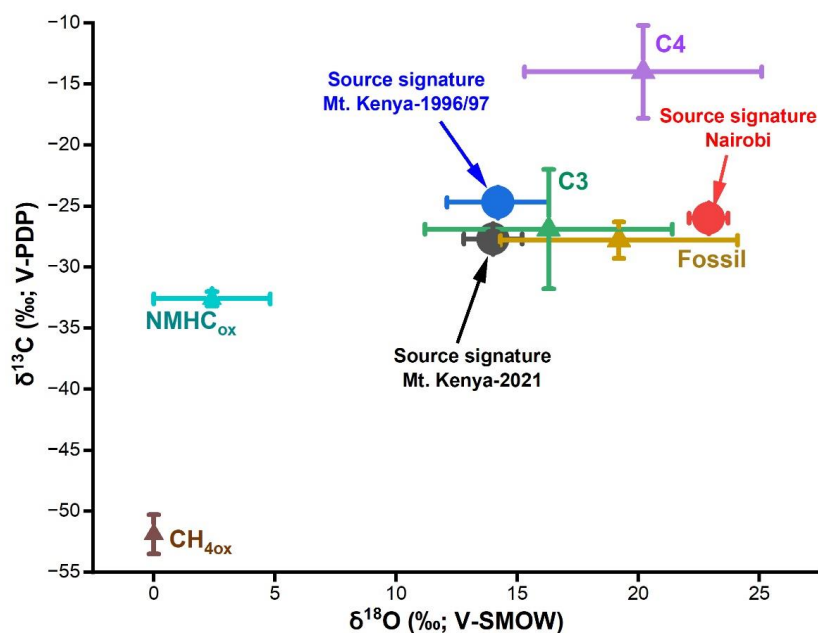
Figure 4: Stable isotope (δ^{13}C and δ^{18}O) source signatures of CO for Nairobi and Mt. Kenya (2021 and 1996/97), and the source end members. The source end members are adopted from Brenninkmeijer et al. (1999)

409
410